Published in final edited form as:

ACS Chem Biol. 2021 June 18; 16(6): 1030–1039. doi:10.1021/acschembio.1c00131.

Mycobacterium tuberculosis PanD structure-function analysis and identification of a potent pyrazinoic acid-derived enzyme inhibitor

Priya Ragunathan[1,#], **Malcolm Cole**[2,#], **Chitra Latka**[1,#], **Wassihun Wedajo Aragaw**[3,#], **Pooja Hegde**[2], **Joon Shin**[1], **Malathy Sony Subramanian Manimekalai**[1], **Sankaranarayanan Rishikesan**[1], **Courtney C. Aldrich**[2,*], **Thomas Dick**[3,4,5,*], **Gerhard Grüber**[1,*]

[1]School of Biological Sciences, Nanyang Technological University, 60 Nanyang Drive, Singapore 637551, Republic of Singapore

[2]University of Minnesota, College of Pharmacy, Department of Medicinal Chemistry 8-101 Weaver-Densford Hall 308 Harvard St. SE, Minneapolis, MN 55455, USA

[3]Center for Discovery and Innovation, Hackensack Meridian Health, 111 Ideation Way, Nutley, New Jersey 07110, USA

[4]Department of Medical Sciences, Hackensack Meridian School of Medicine, 123 Metro Boulevard, Nutley, New Jersey 07110, USA

[5]Department of Microbiology and Immunology, Georgetown University, 3900 Reservoir Road NW Medical-Dental Building, Washington, DC 20007, USA

Abstract

A common strategy employed in antibacterial drug discovery is targeting of biosynthetic processes which are essential and specific for the pathogen. Specificity in particular avoids undesirable interactions with potential enzymatic counterparts in the human host, and ensures on-target toxicity. Synthesis of pantothenate (Vitamine B5), a precursor of the acyl carrier coenzyme A, is an example of such a pathway. In *Mycobacterium tuberculosis (Mtb*), the causative agent of tuberculosis (TB), pantothenate is formed by pantothenate synthase, utilizing D-pantoate and β-Ala as substrates. β-Ala is mainly formed by the decarboxylation of L-aspartate, generated by the decarboxylase PanD, a homo-oligomer in solution. Pyrazinoic acid (POA), the bioactive form of the TB prodrug pyrazinamide, binds and inhibits PanD activity weakly. Here, we generated a library of recombinant *Mtb* PanD mutants based on structural information and PZA/POA resistance mutants. Alterations in oligomer formation, enzyme activity and/or POA binding were

*To whom correspondence should be addressed: Prof. Dr. Courtney Aldrich, aldri015@umn.edu; Prof. Dr. Thomas Dick; Thomas.Dick@hmh-cdi.org; Prof. Dr. Gerhard Grüber, ggrueber@ntu.edu.sg.
#Authors contributed equally to this work

Author contributions. P.R., M.C., C.L., W.W.A., C.A., T.D., and G.G. conceived and designed the experiments. P.R., M.C., C.L., W.W.A., P.H., J.S., M.S.S.M., and S.R. performed the experiments and analyzed the data. P.R., M.C., C.L., W.W.A., J.S., M.S.S.M., C.A., T.D., and G.G. wrote the paper with contribution from other authors.

Conflict of interest. The authors declare that they have no conflicts of interest with the contents of this article.

Supporting Information Available: The supplementary information on PanD mutants' primers, MALDI-TOF, binding affinity studies (ITC/NMR) of WT PanD and mutants with POA or its analogs and the synthetic chemistry adopted in this study are provided. This material is available free of charge *via* the Internet at http://pubs.acs.org.

observed in respective mutants, providing insights into essential amino acids for *Mtb* PanD's proper structural assembly, decarboxylation activity and drug interaction. This information provided the platform for the design of novel POA analogs with modifications at position 3 of the pyrazine ring. Analog 2, incorporating a bulky naphthamido group at this position, displayed a 1,000-fold increase in enzyme inhibition compared to POA, along with moderately improved antimycobacterial activity. The data demonstrate that an improved understanding of mechanistic and enzymatic features of key metabolic enzymes can stimulate design of more potent PanD inhibitors.

Graphical Abstract

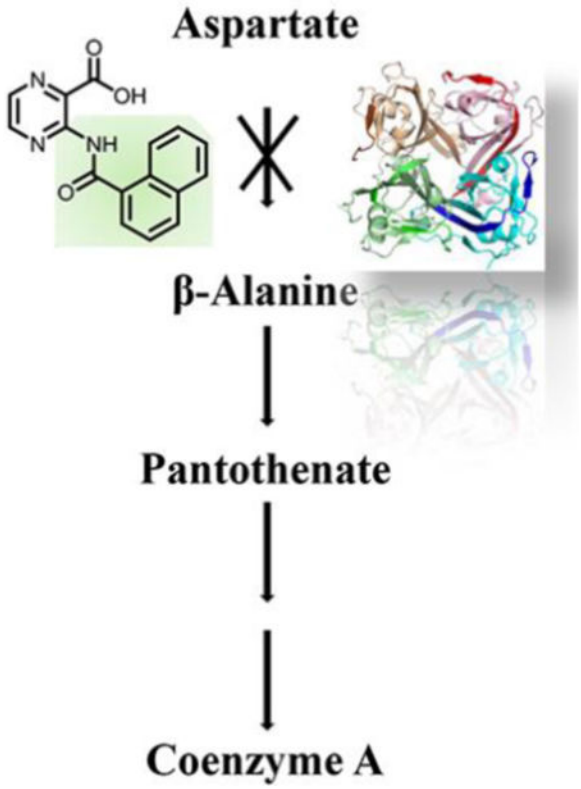

Keywords

Tuberculosis; Mycobacteria; pyrazinamide; pyrazinoic acid; coenzyme A; aspartate decarboxylase

INTRODUCTION

Vitamin B5 (pantothenate) is an essential cofactor involved in a number of critical metabolic processes, including fatty acid synthesis and ATP production (1). Pantothenate is a precursor of 4'-phosphopantotheine, the acyl carrier molecule employed by coenzyme A (CoA) and acyl carrier enzymes (1). *De novo* synthesis of pantothenate is catalyzed in prokaryotes by pantothenate synthase PanC, which promotes condensation of substrates D-pantoate and β-alanine (β-Ala). β-Ala in turn is formed via decarboxylation of L-aspartate (L-Asp), a

reaction catalyzed by the L-Asp α-decarboxylase PanD (2). As pantothenate, like other vitamins, is not synthesized *de novo* by humans, this biosynthetic pathway represents an attractive target for antibacterial drug discovery. The attractiveness of the pathway is supported by the clinical efficacy of pyrazinamide (PZA), an antibiotic active against *Mycobacterium tuberculosis* (*Mtb*), the causative agent of tuberculosis (TB) (3). PZA is a prodrug and converted to its bioactive form pyrazinoic acid (POA) by the PZase/nicotinamidase, encoded by *Mtb pncA* (4). However, *in vitro* whole cell activity of PZA/POA is rather modest and more potent analogs may provide a next generation drug with improved efficacy (5–8). POA interferes with CoA biosynthesis by blocking PanD mediated conversion of asparate to β-Ala (7). Interestingly, POA has a dual on-target mechanism. In addtion to acting as a very weak mM inhibitor of PanD's enzymatic activity (5, 6), binding of POA to PanD promotes degradation of the protein by the caseinolytic protease complex ClpC1-ClpP (6). Besides being involved in POA binding, the C-terminus of *Mtb* PanD plays a key role in ClpC1-ClpP-mediated degradation, as it includes a degradation tag recognized by the protease complex (9, 10).

Biochemical and biophysical studies have revealed that *Mtb* PanD forms an oligomer in solution (5) as well as in the asymmetric unit (a dimer of tetramers) of the first determined crystal structure ((11); PDB ID: 2C45). The enzyme is initially translated as an inactive proenzyme. Activation occurs via cleavage between the N-terminal amino acids G24 and S25, which proceeds via intramolecular nucleophilic addition of the S25 hydroxyl into the neighboring carbonyl, followed by elimination via deprotonation of the S25 α proton (12). The end result of this cleavage is a smaller β-chain (M1-G24) (~3 kDa) and an α-chain (~13 kDa) containing a critical N-terminal pyruvoyl residue [(Pyr25 to I139) (6, 12) (Supplementary Figure 1)]. The N-terminus of one *Mtb* PanD monomer interacts with the C-terminus of an adjacent subunit, enabling oligomerization and binding of POA (Figure 1). Residue K9 appears to be critical in stabilizing subunit association; but the interactions driving oligomerization are not well understood. Possible relevant features include intra-monomer hydrogen bonding interactions between K9 and H11, R104 and V106; and inter-monomer hydrogen bonding with G24 as well as Y58, a residue previously demonstrated essential for POA-binding ((6) PDB ID: 6OYY) (Figure 1). These in part may explain why POA-resistant mutants occur mainly at PanD's termini (13, 14) and that proper oligomer formation is essential for enzyme activity. Interestingly, POA resistance is also observed with substitutions of neighboring residue K7, which has stabilizing intra-monomer interactions with α-chain residues E42, D37, R104 and A89 (Figure 1). Further explorations are required to better understand the role of this residue in enzymatic activity. So far, it remains unclear if POA resistance observed *panD* mutations is caused by: (*a*) subtle movements of the α- and β-chain relative to each other; direct modification of POA-binding residues; perturbations in oligomerization state, (*d*) alterations on the affinity and residence time of POA rather than POA-binding interactions as described for the resistant mutants H21R and M117I (6), and/or (*e*) alteration of PanD's enzyme activity.

POA inhibits PanD-mediated β-Ala production weakly (5), which is in line with its low binding affinity (6). POA binding is driven in part by hydrogen bonding with A74, A75, and R54, as well as other electrostatic interactions within the binding site (5, 6). However, questions remain regarding how POA reaches this binding site, which likely requires

significant conformational alterations of the oligomeric enzyme based on existing structural information (6).

Considering the current structural and mechanistic knowledge regarding the on-target mechanisms of POA, a critical knowledge gap restricting design of more potent *Mtb* PanD inhibitors requires further insight into the most critical amino acids for both mechanistic processes and POA resistance. Here, we used an interdisciplinary approach to gain greater understanding of specific residues critical for PanD's enzymatic activity and characterized altered catalysis of resistant mutant versions of the protein. These insights enabled the design of a novel POA analogue, featuring modification at position 3 of the pyrazine ring, which furnished a 1,000-fold increase in enzyme inhibition compared to the parent molecule.

RESULTS AND DISCUSSION

Effect of N-terminal mutations on oligomer formation and *Mtb* PanD activity

Designing improved inhibitors of *Mtb* PanD requires a deeper understanding of the amino acids essential for catalysis and oligomer formation. Using site-directed mutagenesis, we concentrated our initial efforts on exploration of N-terminal *Mtb* PanD regions of four or more residues that might mediate or disrupt the homodimer interface and, thereby, enzyme catalysis. Lane 2 of Figure 2A and 2B demonstrates that deleting the first 25 N-terminal residues of the $PanD_{25–139}$ mutant altered its oligomeric state into a monomer, reflected by the change of a higher molecular band of the wild-type (WT) enzyme (lane 1) compared to the lower molecular band of the mutant (lane 2). To narrow down the specific residues involved in this process, $PanD_{K9AH11AC17AH21A}$, $PanD_{K9AH11AH21A}$, and $PanD_{K9AH11A}$ mutants were generated. These mutations prevent oligomerization, as demonstrated in Figure 2C and 2D (lanes 5, 6 and 7). A band at ~15 kDa and one above 15 kDa were observed and analyzed by MALDI-TOF, showing that both the bands represent PanD (Supplementary table 3A and 3B) with identical molecular mass. A SDS PAGE is a semi denaturating gel, where different conformations of the same protein lead to different accessibility of charge distribution, resulting in an altered elution within the electric field. We also examined the single mutants $PanD_{K7A}$, $PanD_{K9A}$, $PanD_{H11A}$, $PanD_{T16A}$, $PanD_{T16S}$, $PanD_{C17A}$, and PanDD31E to explore the effect of individual amino acid substitutions on oligomerization potential. Interestingly, none of the mutants had an effect on the oligomeric state of PanD except for $PanD_{K9A}$ (Figure 2).

Possible enzymatic alterations caused by these N-terminal *Mtb* PanD mutants were studied by directly observing PanD-mediated conversion of L-Asp to β-Ala using ^{1}H NMR spectroscopy. The formation of β-Ala from L-Asp was monitored and quantified by peak volume of the generated side-chain doublet of β-Ala at ~2.5 ppm after 40 min of incubation. As revealed in Figure 3, all PanD mutants showed decreased enzyme activity compared to WT PanD. In line with the previously observed oligomerization results, the truncated α-chain $PanD_{25–139}$, as well as mutants $PanD_{K9A/H11A/C17A/H21A}$, $PanD_{K9A/H11A/H21A}$, and $PanD_{K9A/H11A}$ were enzymatically inactive. importantly, this was also observed for the single mutants $PanD_{K9A}$ and $PanD_{H11A}$, underlining their essential role in *Mtb* PanD's enzyme activity. In addition, partially decreased enzyme activity was observed for Pan_{DK7A},

$PanD_{T16A}$, $PanD_{T16S}$ and $PanD_{D31E}$, indicating that these residues have an effect on enzyme catalysis. Interestingly, $PanD_{T16A}$ showed a higher conversion rate as compared to $PanD_{T16S}$. The difference between $PanD_{T16A}$ and $PanD_{T16S}$ might be caused due to changes of a local hydrogen bonding, hydrophobic interaction network and/or structural alteration due to the mutation of T16. Finally, $PanD_{C17A}$ shows almost 90% enzyme activity when compared to PanD WT, indicating that C17 is not a critical residue for L-Asp decarboxylation.

Characterization of recombinant *Mtb* PanD harboring mutations in the C-terminal region

Current structural information on *Mtb* PanD suggests the C-terminal residues form loops that cover the active site region (6). C-terminal mutations have been reported from PZA-resistant *Mtb* strains isolated both *in vitro* (13, 15, 16) and *in vivo* (7, 15, 17). Examples are the mutants H119N and E126A, which are present in multidrug-resistant (MDR) *Mtb* clinical isolates (18), or the nonsense mutation in E126, observed in *in vitro*-isolated drug resistant strains of *Mtb* (5, 15). In addition, L132P and P134S have also been reported as mutations conferring resistance against PZA in clinical isolates of *Mtb* (7, 17). Here, we generated the recombinant *Mtb* PanD mutants H119N, E126A, L132P and P134S and observed that the enzyme activity of mutant $PanD_{E126A}$ and $PanD_{P134S}$ decreased by about 85% and 87%, respectively, indicating a role of these C-terminal residues in L-Asp to β-Ala transformation (Figure 4A). In comparison, the overall decrease in enzyme activity was lower in $PanD_{H119N}$ and $PanD_{L132P}$ (~25% and ~50%, respectively). These results are in line with a different band pattern of the mutants $PanD_{E126A}$ and $PanD_{P134S}$ in Figure 4C, (lane 3, 5), when compared to the mutants $PanD_{H119N}$ and $PanD_{L132P}$, a pattern comparable to the one explained earlier as in figure 2C. Interestingly, for all the four C-terminal mutants studied, a significant line broadening of the NMR spectra was observed, reflecting intermediate exchange between the substrate L-Asp and the product β-Ala during enzymatic reaction. It is to note that different oligomeric states of the mutants could also contribute to the line broadening of L-Asp and the β-Ala peaks by increasing molecular tumbling rates due to mixed population of oligomeric states of each mutant.

Mutations in *Mtb* PanD eliminate binding of POA

Next, we used our ensemble of N- and C-terminal *Mtb* PanD mutants to test their influence on POA-binding via isothermal titration calorimetry (ITC). As shown in Supplementary Figure 2 and Supplementary Table 1, no binding was observed for the mutants $PanD_{K9A/H11A/C17A/H21A}$, $PanD_{K9A/H11A/H21A}$, $PanD_{K9A/H11A}$, and the single mutant $PanD_{K9A}$ (Supplementary Figure 3). Strikingly, all these isoforms showed alterations in both oligomeric state (Figure 2) and enzyme activity (Figure 3). No binding of the drug was detected for the single amino acid substitution mutant $PanD_{H11A}$, which did not affect oligomerization but was nearly enzymatically inactive. While a reduction in POA-binding affinity was observed for $PanD_{K7A}$ (123 ± 0.3 μM) and $PanD_{T16A}$ (184 ± 0.8 μM), the K_D-values of the remaining single mutants ($PanD_{C17A}$, $PanD_{D31E}$, $PanD_{E126A}$, and $PanD_{L132P}$) were comparable to WT PanD (20 ± 0.2 μM) (Supplementary Figure 3 & 4). The presented analysis of PanD mutants suggests that subtle protein modifications can affect POA potency in a number of ways, including reducing affinity to the drug, altering the oligomeric state and/or activity of the target enzyme.

POA analogs with alterations at position 3 of the pyrazine ring potently inhibit β-Ala production

The mutant studies highlight the essentiality of residues K9 and H11 for PanD function. As shown in the structure of *Helicobacter pylori* PanD complex (Supplementary Figure 5A), the substrate analog isoasparagine is in 2.63 Å from the lysine residue and proposed to be involved in the enzyme–substrate with Schiff base intermediate (19). *Mtb's* PanD residue K9 participates in a number of hydrogen bonding interactions with neighboring residues, including intra-monomeric interactions with H11, R104 and V106, as well as interactions with Y58 and G24 of the adjacent subunit in the dimer interface (Supplementary Figure 5B). A closer look at the POA-bound *Mtb* PanD structure (Supplementary Figure 5B; 6) reveals only a van der Waals interaction with POA, leaving considerable space within the binding pocket between position 3 of the pyrazine ring of POA and the catalytically essential residues K9 and H11. We hypothesized that functionalization at this 3-position might better fill this binding pocket, improving binding, while also disrupting enzyme activity through greater interactions with these critical active site residues. To test our hypothesis, a series of analogs at position 3 were synthesized (see Supplementary Information) and profiled using PanD enzyme activity and ITC assays.

Five analogs (1–5) displayed binding comparable to POA (K_D = 20 ± 0.5 μM) (Supplementary Figure 6) with K_D values between 15 ± 0.5 μM to 50 ± 3.2 μM (Table 1), while analogs 6 to 11 and 12 to 18 showed low or no binding, respectively (Table 1). To test whether analogs 1–5 have comparable or increased inhibitory potency in enzymatic conversion of L-Asp to β-Ala, ^{1}H-NMR titration experiments of these analogs with *Mtb* PanD were performed. As described recently (6, 9) and confirmed in Figure 5, POA shows poor inhibition (4.8%) of β-Ala production at a concentration of 200 μM. In comparison analog 1, 3, 4 and 5 showed an inhibition of 15.1%, 25.3%, 13.5%, and 64.3%, respectively (Supplementary Figure 7). Importantly, 200 μM of analog 2, 3-(1-naphthamido) pyrazine-2-carboxylic acid, inhibited enzymatic activity by 95.5%. The concentration dependent enzyme assays of analog 2 resulted in enzyme inhibition of about 50% at 2.5 μM (Figure 5), a 1,000-fold enhancement in enzyme inhibition compared to POA. The potency of analog 2 was comparable when dissolved in deuterated DMSO (*d*6-DMSO) or in buffer (Supplementary Figure 8), indicating favorable solubility characteristics.

Seeking to clarify the relationship between the structure of analog 2 and its increased inhibitory effect against PanD, related analogues 19 and 20 containing bulky, hydrophobic substituents at the 3-position were synthesized and their inhibition of β-Ala production was tested. Supplementary Figure 7 demonstrates that both analogs 19 and 20 have a better inhibitory effect at 200 μM (74.6% and 69.9%, respectively) compared to POA. The data demonstrate nicely that extending position 3 of the pyrazine moiety significantly improves PanD inhibition.

In addition to (weakly) inhibiting enzymatic activity of recombinant PanD, binding of POA to PanD has been shown to trigger ClpC1-ClpP-dependent degradation of the protein (9). To determine whether analog 2 retained POA's 'degrader activity', we tested the effect of the analog on the intra-bacterial levels of PanD employing a Red fluorescence protein – PanD reporter strain of *M. bovis* BCG (9). Treatment of cultures with POA caused a reduction of

intra-bacterial PanD as reported previously (Figure 6A-B; 9). Surprisingly, the more potent enzyme inhibitor analog 2 showed only a weak, if any effect on intra-bacterial PanD levels (Figure 6A-B). This result suggests that analog 2 acts largely via one on-target mechanism, enzyme inhibition, whereas POA displays dual on-target mechanisms, enzyme inhibition and promoting degradation. We a also sought to explore the role of our novel analog on PanD oligomerization. *Mtb* PanD was incubated with POA or analog 2, and then oligomerization was assessed using electrophoresis (as employed previously for the PanD mutants). Figure 6C shows that POA alters the oligomerization of *Mtb* PanD. POA-induced oligomerization has recently been visualized by electron microscopy and biophysical studies, and appears to be required for enhanced PanD degradation by ClpC1–ClpP (9). This effect may in part also explain why *Mtb* PanD could not be co-crystallized in the presence of POA (6). Consistent with the lack of PanD degradation promoting activity of analog **2**, no major oligomerization change of *Mtb* PanD was observed in the presence of the analog. Thus, inhibition of *Mtb* PanD by analog 2 appears to be due to silencing the events inside the catalytic center of the enzyme and is not related to major quaternary structural changes of PanD.

To determine the effect of the increased PanD enzyme inhibition activity and the loss of the PanD degradation promoting activity of analog 2 on its whole cell growth inhibition activity, MIC assays were conducted against *M. bovis* BCG, an attenuated variant of *Mtb* (20). As shown in figure 7A, analog 2 showed antibacterial whole cell activity and in fact displayed a moderate 4-fold improvement in MIC_{50} (200 μM) compared to POA (MIC_{50} 800 μM). The POA-like whole cell activity of analog 2 suggests that the improved enzyme inhibition activity of the analog compensates for the loss of its target degradation inducing activity.

Analog 2 do not display uncoupler activity

POA has been described to be an uncoupler and to disrupt the proton motive force with the consequence of lowering cellular ATP levels (21–23). Thus, we tested whether analog 2 may affect the proton motive force. Employing *M. smegmatis* inverted membrane vesicles (IMVs; see Materials and Methods), analog 2 up to 1 mM did not affect the membrane potential (Figure 7B). Thus, analog 2 do not display any uncoupling activity.

CONCLUSION

In this study, we presented insights into *Mtb* PanD residues critical for catalysis as well as oligomer formation and demonstrated that some *panD* mutations observed in PZA/POA-resistant *Mtb* strains showed altered oligomer and enzymatic activities in recombinant *Mtb* PanD mutant proteins. Guided by structural insights, novel POA analogs were designed featuring modifications at position 3 of the pyrazine ring to increase disruption of the critical catalytic residues of *Mtb* PanD. The most potent analog 2 (3-(1-naphthamido)pyrazine-2-carboxylic acid) displayed a 1,000-fold enhancement in enzyme inhibition compared to POA. In contrast to POA, which appears to block the PanD catalyzed step largely by promoting PanD's degradation by the ClpC1-ClpP-complex (9), the effect of analog 2's inhibition of *Mtb* PanD appears to be mainly due to silencing the conversion of L-Asp to β-Ala. Thus, the dual on-target activities observed for POA, enzyme inhibition and promotion

of target degradation, appear to be separable. The moderately improved MIC potency demonstrates that an improved understanding of mechanistic and enzymatic features of key metabolic enzymes can stimulate design of more potent enzyme inhibitors. This exciting result further validates similar mechanistic studies as a robust starting point for the development of new molecules in the fight against TB and other infectious diseases plaguing the world today.

MATERIALS AND METHODS

Cloning, production and purification of *Mtb PanD* mutants

The construct $panD_{25–139}$ was amplified using the primers shown in the Supplementary Table 1. The amplified products were ligated into the pET9-d1-His6 vector (24). The coding sequences for the constructs were verified by DNA sequencing. The final plasmids were subsequently transformed into *Escherichia coli* BL-21 (DE3) cells (Stratagene).

Constructs of cumulative *panD* mutants, $panD_{K7A}$, $panD_{K9A}$, $panD_{H11A}$, $panD_{C17A}$, $panD_{T16A}$, $panD_{T16S}$, $panD_{D31E}$, $panD_{H119N}$, $panD_{E126A}$, $panD_{L132P}$, $panD_{P134S}$, $panD_{K9AH11A}$, $panD_{K9AH11AH21A}$, $panD_{K9AH11AC17AH21A}$ were created through the In-Fusion strategy (25) with Hi-Fi KAPA DNA polymerase (KAPA Biosystems, USA) which involves a series of PCRs with specially designed primers (Supplementary Table 1) each pair having an approximately 15-bp overlap that incorporates the desired mutation. The plasmid DNA from pET9d-*MbpanD*, which is identical in its amino acids sequence to *Mtb* PanD, was used as a template for amplifying *panD* with primers having desired mutations. The PCR product was treated with DpnI before direct transformation into electro-competent *E. coli* DH5α cells to be circularized as plasmids. Likewise, the plasmid was extracted and sent for DNA sequencing to check that the intended mutation had been introduced. Once verified, the plasmid served as the template in the subsequent PCR for the next construct. This process was repeated until all the constructs of *panD* mutants were obtained. The plasmids were then transformed into *E. coli* BL21 (DE3) cells for protein production. All the *panD* mutants were expressed and purified by the method described earlier (5).

Isothermal Titration Calorimetry

ITC experiments were carried out with an ITC200 microcalorimeter (MicroCal, Northampton, UK), to study the binding of PanD mutants with POA or binding of newly synthesized POA analogs as recently described (5).

^{1}H-1D NMR studies of L-Asp to β-Ala conversion

NMR samples containing 2 mM L-Asp, 10 μM WT PanD or PanD mutants were prepared in 20 mM sodium phosphate buffer (pH 6.5) in deuterated water. Basic ^{1}H-1D NMR spectra were collected with pre-saturation of solvent water (relaxation delay 2 s; solvent pre-saturation applied during the relaxation delay) after 40 min incubation of NMR sample using a Bruker Avance 400 MHz NMR spectrometer, equipped on a 5 mm BBI probe head at 298 K. The inhibitory effect of the analogs, dissolved in *d*6-DMSO or for comparison in buffer (20 mM sodium phosphate buffer (pH 6.5)) were added into the enzymatic reaction mixture at a final concentration of 0, 2.5, 10, 100, 200 and 500 μM of the respective analog. After 40

min incubation at 298 K, a series of ^{1}H-1D spectra were obtained and the inhibition rate at each concentration of the analogs was calculated by measuring the peak volume of the product β-Ala. In comparison, a ^{1}H-1D NMR spectra was recorded in the presence of 200 μM of POA. DSS 2,2-Dimethyl-2-silapentane-5-sulfonate) was used as internal standard for the calibration of the NMR peaks.

Minimum inhibitory concentration determination and PanD reporter assay

The growth inhibition dose-response assay for *M. bovis* BCG (ATCC 35734) and *M. tuberculosis* H37Rv (ATCC 27294) was carried out using the broth microdilution method, as described previously (26). The PanD reporter assay was performed according to Gopal et al. using a *M. bovis* BCG strain harbouring a constitutively expressed red fluorescent protein – PanD fusion (9).

Test of possible uncoupling of IMVs

A possible uncoupler effect of analog **2** on *M. smegmatis* mc^{2} 155 IMVs was measured on the basis of a decrease in ACMA fluorescence using a Cary Eclipse fluorescence spectrophotometer (Varian Inc., Palo Alto, CA) as described previously (27, 28).

Supplementary Material

Refer to Web version on PubMed Central for supplementary material.

Acknowledgements.

Research reported in this publication is supported by the National Institute of Allergy and Infectious Diseases of the National Institutes of Health under Award Number R01AI106398 (T.D., C.A., G.G.) the National Research Foundation (NRF) Singapore, NRF Competitive Research Programme (CRP), Grant Award Number NRF–CRP18–2017–01) to G.G., and the Singapore Ministry of Education Academic Research Fund Tier 1 (RG107/20) to GG.

REFERENCES

1. Vagelos PR (1973). Acyl group transfer. In The Enzymes (Boyer PD, ed.), pp. 155–199, Academic Press, New York.
2. Dusch N, Puhler A and Kalinowski J (1999) Expression of the Corynebacterium glutamicum panD gene encoding L-aspartate-α-decarboxylase leads to pantothenate overproduction in Escherichia coli. Appl. Environ. Microbiol 65, 1530–1539. [PubMed: 10103247]
3. Malone L, Schurr A, Lindh H, McKenzie D, Kiser JS and Williams JH (1952) The effect of pyrazinamide (aldinamide) on experimental tuberculosis in mice. Am. Rev. Tuberc 65, 511–518. [PubMed: 14924173]
4. Scorpio A and Zhang Y (1996) Mutations in pncA, a gene encoding pyrazinamidase/nicotinamidase, cause resistance to the antituberculous drug pyrazinamide in tubercle bacillus. Nat. Med 2, 662–667. [PubMed: 8640557]
5. Gopal P, Nartey W, Ragunathan P, Sarathy J, Kaya F, Yee M, Setzer C, Manimekalai MSS, Dartois V, Grüber G. and Dic T. (2017) Pyrazinoic Acid Inhibits Mycobacterial Coenzyme A Biosynthesis by Binding to Aspartate Decarboxylase PanD. ACS Infect Dis 10, 807–819.
6. Sun Q, Li X, Perez LM, Shi W, Zhang Y and Sacchettini JC (2020) The molecular basis of pyrazinamide activity on Mycobacterium tuberculosis PanD. Nat. Comm 11:339, 10.1038/s41467-019-14238-3.
7. Zhang Y, Shi W, Zhang W and Mitchison D (2013) Mechanisms of pyrazinamide action and resistance. Microbiol Spectr 2, 1–12. [PubMed: 25530919]

8. Lamont EA, Dillon NA and Baughn AD (2020) The Bewildering Antitubercular Action of Pyrazinamide. Microbiol. Mol. Biol. Ev 84: e00070–19.doi 10.1128/MMBR.00070-19.
9. Gopal P, Sarathy JP, Yee M, Ragunathan P, Shin J, Bhushan S, Zhu J, Akopian T, Kandror O, Lim TK, Gengenbacher M, Lin Q, Rubin EJ, Grüber G and Dick T (2020) Pyrazinamide triggers degradation of its target aspartate decarboxylase. Nat. Commun 11, 1661; doi: 10.1038/s41467-020-15516-1. [PubMed: 32245967]
10. Gopal P, Grüber G, Dartois V and Dick T (2019) Pharmacological and Molecular Mechanisms Behind the Sterilizing Activity of Pyrazinamide. Trends Pharmacol Sci 40, 930–940. [PubMed: 31704175]
11. Gopalan G, Chopra S, Ranganathan A and Swaminathan K (2006) Crystal structure of uncleaved L-Aspartate-α-decarboxylase from Mycobacterium tuberculosis. PROTEINS: Structure, Function, and Bioinformatics 65, 796–802.
12. Chopra S, Pai H, Ranganathan A. (2002) Expression purification and biochemical characterization of Mycobacterium tuberculosis aspartate decarboxylase, ADC. Protein Expr Purif 25, 533–540. [PubMed: 12182836]
13. Gopal P, Tasneen R, Yee M, Lanoix JP, Sarathy J, Rasic G, Li L, Dartois V, Nuermberger E and Dick T (2017) In vivo-selected pyrazinoic acid resistant Mycobacterium tuberculosis strains harbor missense mutations in the aspartate decarboxylase PanD and the unfoldase ClpC1. ACS Infect. Dis 3, 492–501. [PubMed: 28271875]
14. Gopal P, Yee M, Sarathy J, Low JL, Sarathy JP, Kaya F, Dartois V, Gengenbacher M and Dick T (2016) Pyrazinamide resistance is caused by two distinct mechanisms: prevention of Coenzyme A depletion and loss of virulence factor synthesis. ACS Infect. Dis 2, 616–626. [PubMed: 27759369]
15. Shi W, Chen J, Feng J, Cui P, Zhang S, Weng X, Zhang W and Zhang Y (2014) Aspartate decarboxylase (PanD) as a new target of pyrazinamide in Mycobacterium tuberculosis. Emerg. Microbes Infect 3, e58.
16. Zhang S, Chen J, Shi W, Liu W, Zhang W and Zhang Y (2013) Mutations in panD encoding aspartate decarboxylase are associated with pyrazinamide resistance in Mycobacterium tuberculosis. Emerg. Microbes Infect 2, e34. [PubMed: 26038471]
17. Hameed HA, Tan Y, Islam MM, Lu Z, Chhotaray C, Wang S, Liu Z, Fang C, Tan S, Yew WW, Zhong N, Liu J and Zhang T (2020) Detection of Novel Gene Mutations Associated with Pyrazinamide Resistance in Multidrug-Resistant Mycobacterium tuberculosis Clinical Isolates in Southern China. Infect. Drug Resist 22, 217–227.
18. Stoffels K, Mathys V, Fauville-Dufaux M, Wintjens R and Bifani P (2012) Systematic analysis of pyrazinamide-resistant spontaneous mutants and clinical isolates of Mycobacterium tuberculosis. Antimicrob. Agents Chemother 56, 5186–5193. [PubMed: 22825123]
19. Lee BI and Suh SW (2004) Crystal Structure of the Schiff Base Intermediate Prior to Decarboxylation in the Catalytic Cycle of Aspartate α-Decarboxylase. J. Mol. Biol 340, 1–7. [PubMed: 15184017]
20. Brosch R, Gordon SV, Garnier T, Eiglmeier K, Frigui W, Valenti P, Dos Santos S, Duthoy S, Lacroix C, Garcia-Pelayo C et al. (2007) Genome plasticity of BCG and impact on vaccine efficacy. Proc. Natl. Acad. Sci. USA 104, 5596–5601. [PubMed: 17372194]
21. Fontes FL, Peters BJ, Crans DC, Crick DC (2020) The acid-base equilibrium of Pyrazinoic acid drives the pH dependence of pyrazinamide-induced Mycobacterium tuberculosis growth inhibition, ACD. Infect. Dis 6, 3004–3014.
22. Lu P, Haagsma AC, Pham H, Maaskant JJ, Mol S, Lill H, Bald D (2011) Pyrazinoic Acid Decreases the Proton Motive Force, Respiratory ATP Synthesis Activity, and Cellular ATP Levels. Antimicrob. Agents Chemother 55, 5354–5357. [PubMed: 21876062]
23. Peterson ND, Rosen BC, Dillon NA, Baughn AD (2015) Uncoupling environmental pH and intrabacterial acidification from pyrazinamide susceptibility in Mycobcaterium tuberculosis. Antimictob. Agents Chemother 59, 7320–7326.
24. Grüber G, Godovać-Zimmermann J, Link TA, Coskun Ü, Rizzo VF, Betz C and Bailer SM (2002) Expression, purification and characterization of subunit E, an essential subunit of the vacuolar ATPase. Biochim. Biophys. Res. Comm 298, 383–391.

25. Raman M and Martin K (2014) One solution for cloning and mutagenesis: In-Fusion®HD Cloning Plus, Nat Methods 11, 972. [PubMed: 25317449]

26. Gengenbacher M, Rao SP, Pethe K and Dick T (2010) Nutrient-starved, non-replicating Mycobacterium tuberculosis requires respiration, ATP synthase and isocitrate lyase for maintenance of ATP homeostasis and viability. Microbiology 156, 81–87. [PubMed: 19797356]

27. Haagsma AC, Driessen NN, Hahn MM, Lill H and Bald D (2010) ATP synthase in slow- and fast-growing mycobacteria is active in ATP synthesis and blocked in ATP hydrolysis direction. FEMS Microbiol. Lett 313, 68–74. [PubMed: 21039782]

28. Hotra A, Suter M, Biuković G, Ragunathan P, Kundu S, Dick T and Grüber G (2016) Deletion of a unique loop in the mycobacterial F-ATP synthase gamma subunit sheds light on its inhibitory role in ATP hydrolysis-driven H(+) pumping. FEBS J 283, 1947–1961. [PubMed: 26996828]

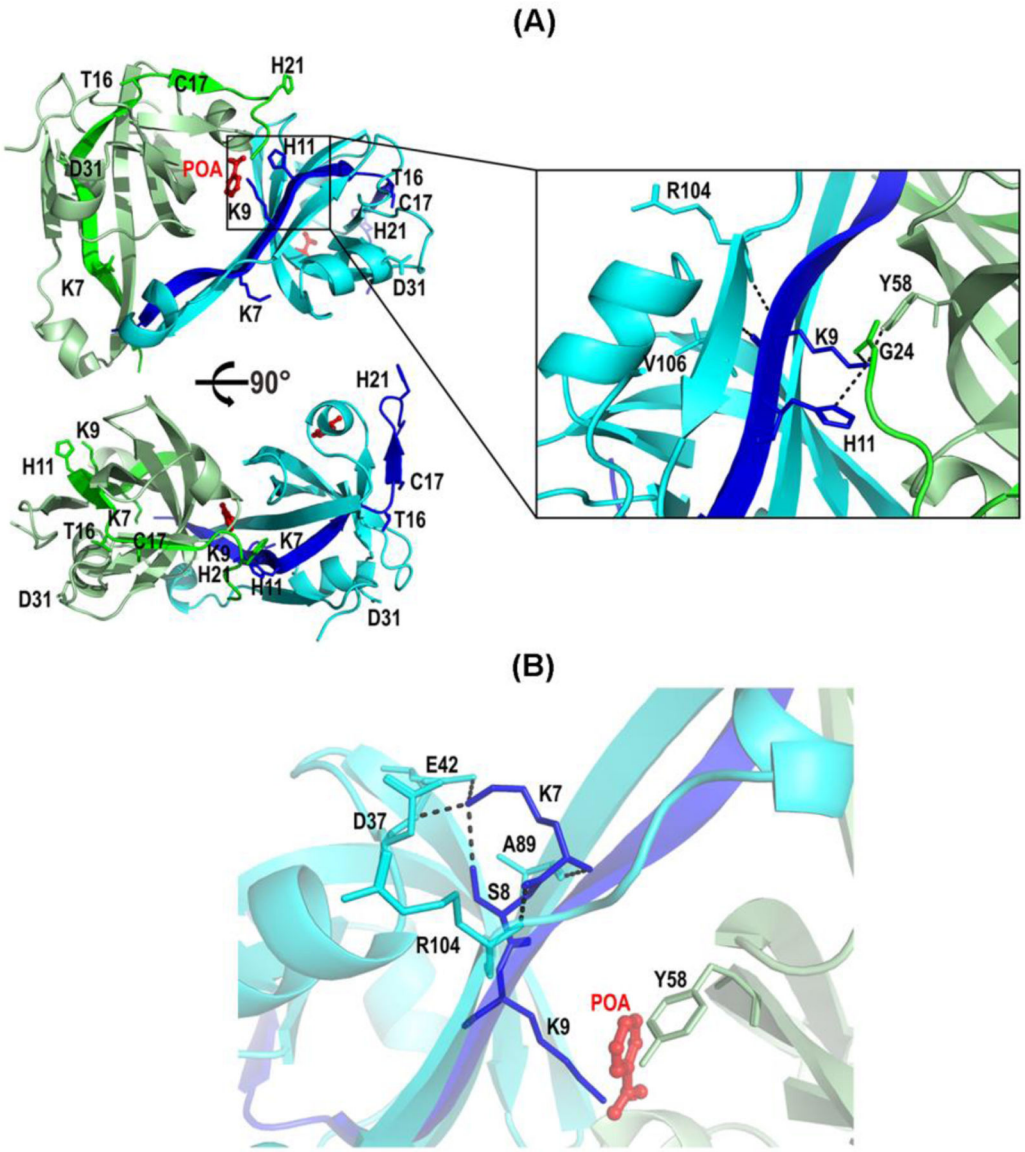

Figure 1:

(A) The N-terminal mutant residues that are used in this study are highlighted in the structure of the *Mtb* PanD dimer (6OYY; 17) which shows the spatial arrangement of the residues. The subunits are shown in *pale green*/*green* and *cyan*/*blue* colors. *Inset* reveals the interaction of K9 with H11, V106 and R104 of the same subunit and Y58 and G24 of the adjacent subunit. (B) Interaction of residue K7 with the same subunit. K7 has side chain interaction with E42, D37 and S8 and main chain interaction with R104 and A89.

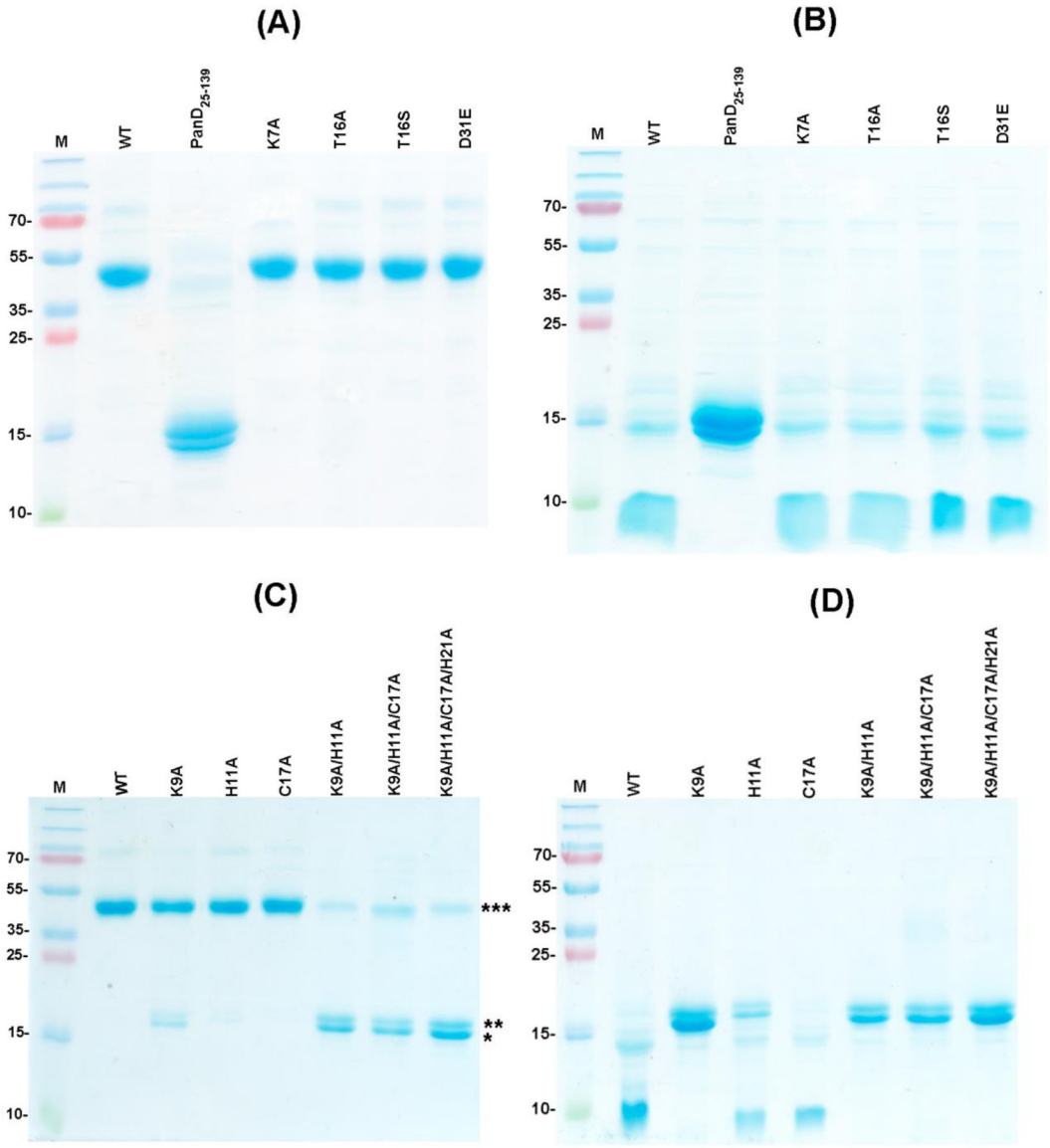

Figure 2:

SDS gels showing the change in the oligomeric states of *Mtb* PanD mutants as compared to WT PanD in presence of DTT (*A*, *C*), and in presence of DTT and heating (*B*, *D*). In figure 2A and 2B, *M*- Marker, *lane 1*- WT PanD, *lane 2*- $PanD_{25–139}$, *lane 3*- $PanD_{K7A}$, *lane* 4- $PanD_{T16A}$, *lane* 5- $PanD_{T16S}$, and *lane* 6- $PanD_{D31E}$. In figure 2C and -D, *M*- Marker, *lane 1*- WT PanD, *lane* 2- $PanD_{K9A}$, *lane3*- $PanD_{H11A}$, *lane 4*- $PanD_{C17A}$, *lane 5*- $PanD_{K9AH11A}$, *lane* 6- $PanD_{K9AH11AH21A}$, and *lane 7*- $PanD_{K9AH11AC17AH21A}$. *- 15 kDa and **- above 15 kDa, represent a monomer of PanD with identical molecular mass as shown by MALDI-TOF (see Supplementary table 3A and 3B), and***- ≥50 kDa, oligomeric form of PanD.

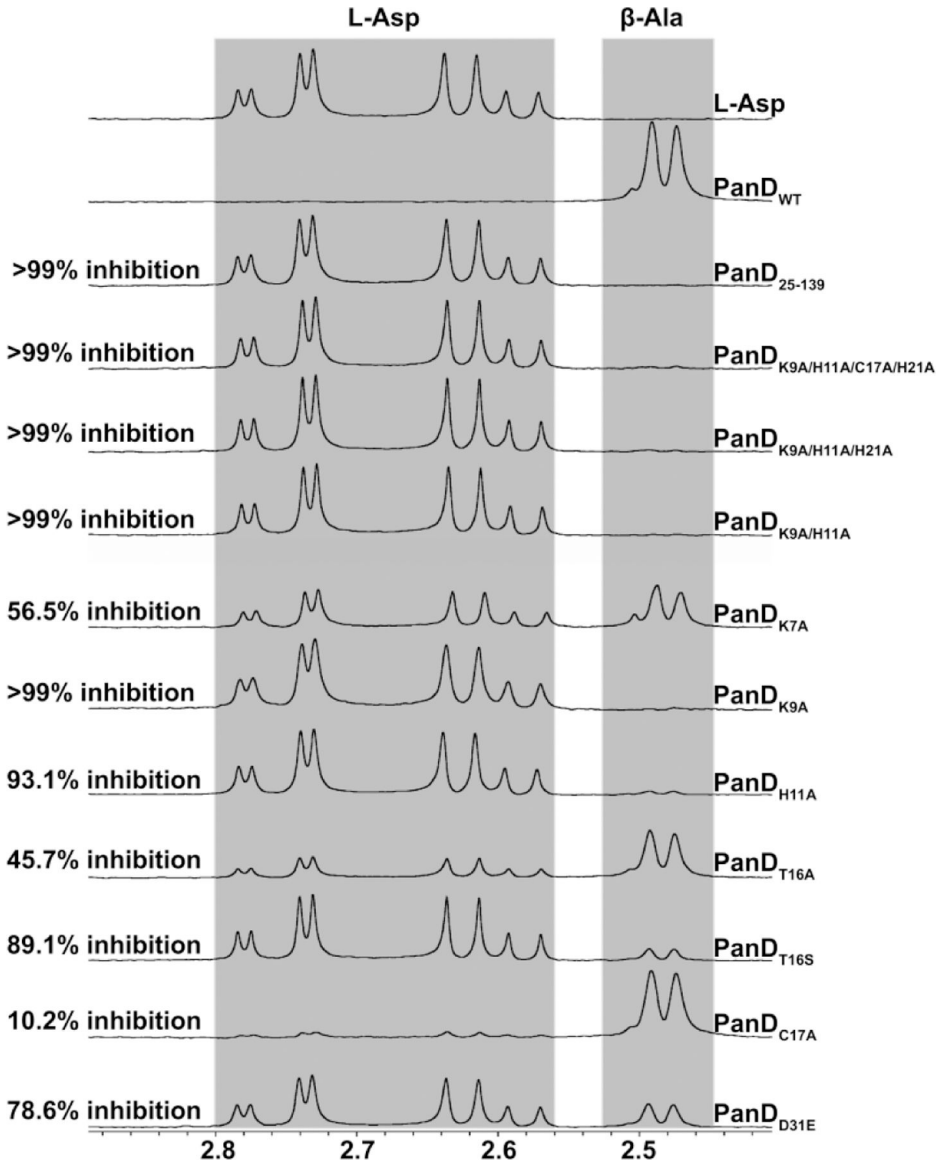

Figure 3:

Representative ^{1}H-1D NMR spectra illustrating the influence of N-terminal mutations on enzymatic conversion of L-Asp to β-Ala. The side chain NMR resonance of substrate L-Asp and product β-Ala are displayed in grey boxes.

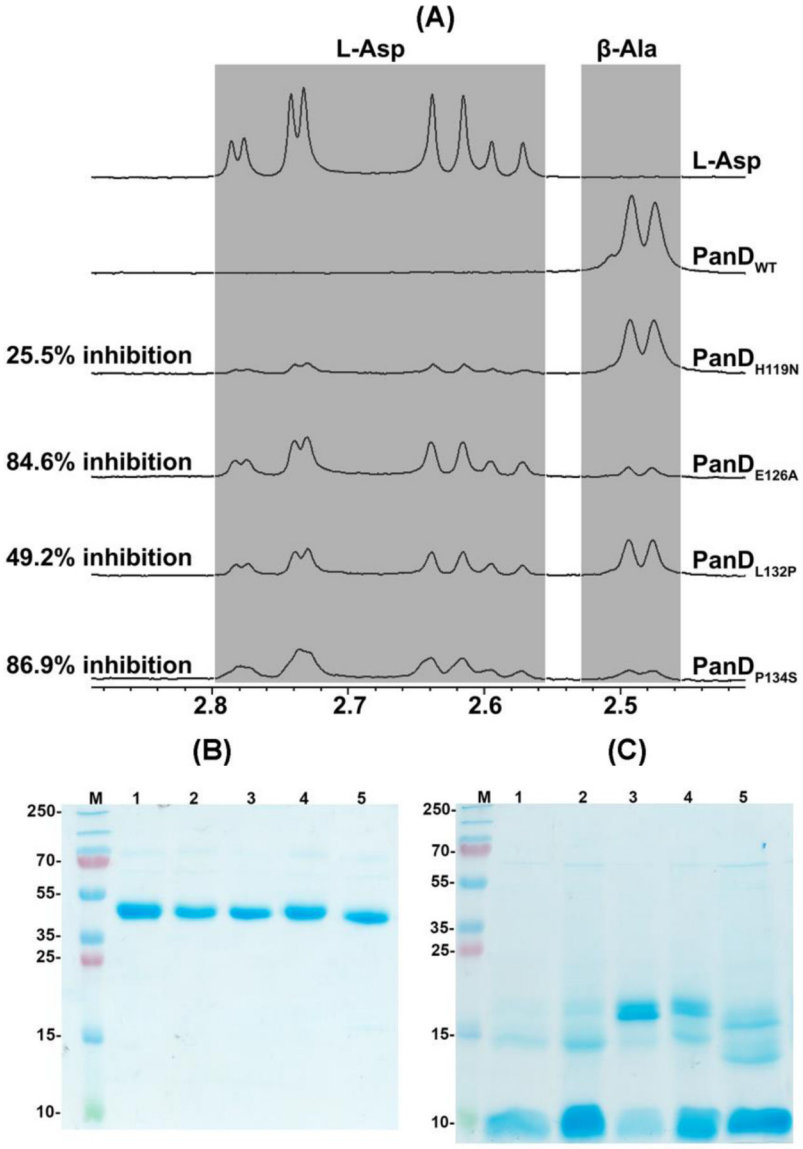

Figure 4:

Effect of C-terminal mutations on *Mtb* PanD's activity and oligomerization. (*A*) Change of enzymatic activity of WT *Mtb* PanD due to C-terminal mutations. Representative ^{1}H-1D NMR spectra show reduction in enzymatic conversion of L-Asp to β-Ala of four C-terminal PanD mutants. WT *Mtb* PanD and selected C-terminal mutants were run on a 17% SDS-PAGE in presence of DTT without heating (*B*) and in presence of DTT and heating (*C*). Changes in oligomerization of PanD are visualized upon introduction of mutations in the C-terminal regions of PanD. *M*- Marker, *lane* 1- WT PanD, *lane* 2- PanD$_{H119N}$, *lane* 3- PanD$_{E126A}$, *lane* 4-PanD$_{L132P}$, *lane* 5- PanD$_{P134S}$.

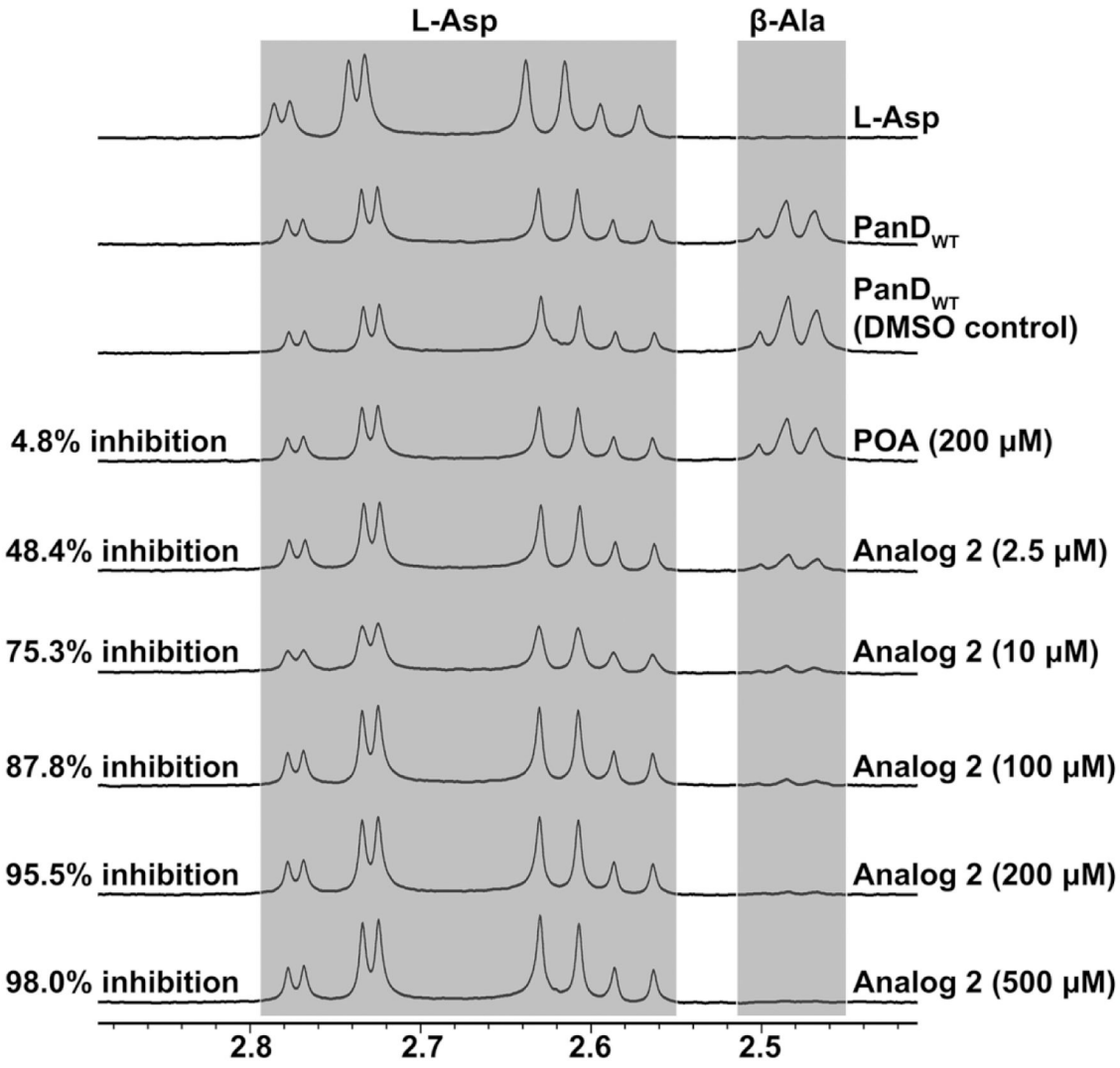

Figure 5:

Inhibitory effect of analog 2 on *Mtb* PanD enzyme activity measured by ^{1}H-1D-NMR. A series of ^{1}H-1D NMR spectra were obtained in the absence and presence of 2.5, 10, 100, 200 and 500 μM of analog 2 after 40 min incubation at 298K. For identification of the effect of solvent DMSO used to dissolve analog 2, 10 μl of *d*6-DMSO was added as positive control in the absence of analog 2. In comparison, an ^{1}H-1D NMR spectra is presented in the presence of 200 μM of POA. The inhibition rate of *Mtb* PanD activity by POA and analog 2 after reaction is displayed in each NMR spectra.

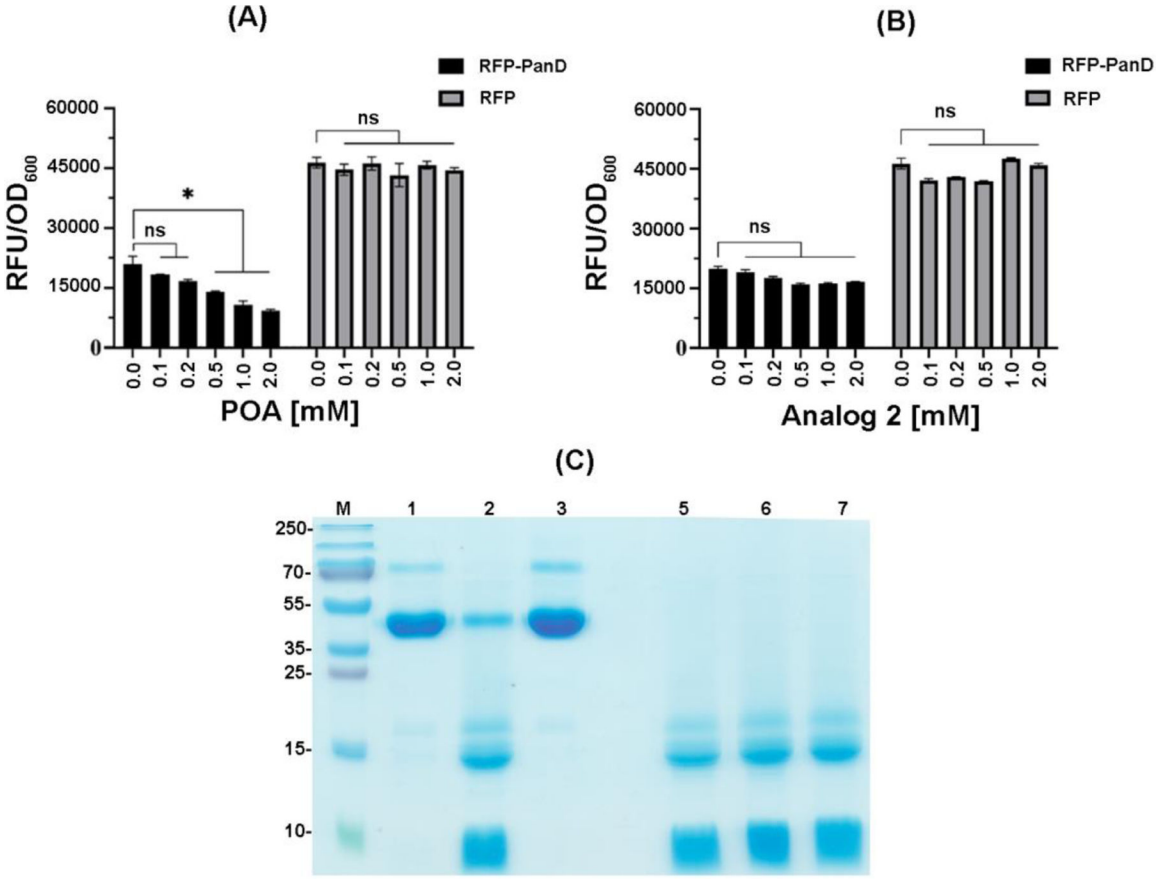

Figure 6:

Effect of pyrazinoic acid (POA) and analog 2 on intrabacterial level of red fluorescence protein (RFP)-PanD fusion protein expressed in *M. bovis* BCG. (*A*) Effect of POA treatment. (*B*) Effect of analog 2 treatment. RFP-PanD: PanD was translationally fused to RFP and constitutively expressed from plasmid pMV262 in *M. bovis* BCG (10). Exponential phase reporter cultures (OD600 = 0.2) were treated with increasing concentrations of POA (*A*) or analog 2 (*B*) for 24 h and fluorescence levels (RFU, relative fluorescence units) were determined as a measure of fusion protein level. RFP: *M. bovis* BCG cultures constitutively expressing RFP without fused PanD (10). Experiments were carried out three times independently with two technical replicates each. Mean values and standard deviations are shown. *indicates a significant difference from the untreated control via the unpaired t test, GraphPad Prism, with a p value of <0.05. ns: not significant. (*C*) Native PanD was incubated with 2 mM POA and 2 mM analog 2 at 298K for 40 min and loaded on a 17% SDS gel in presence of DTT without heating and in presence of DTT with heating. In accordance with our previously published data, POA leads to degradation of PanD unlike analog 2. *M*-Marker, *lane 1*- WT PanD unheated, *lane 2*- PanD + 2 mM POA unheated, *lane 3*- PanD + 2 mM analog 2 unheated, *lane 5* WT PanD heated, *lane* 6- PanD + 2 mM POA heated, *lane* 7- PanD + 2 mM analog 2 heated.

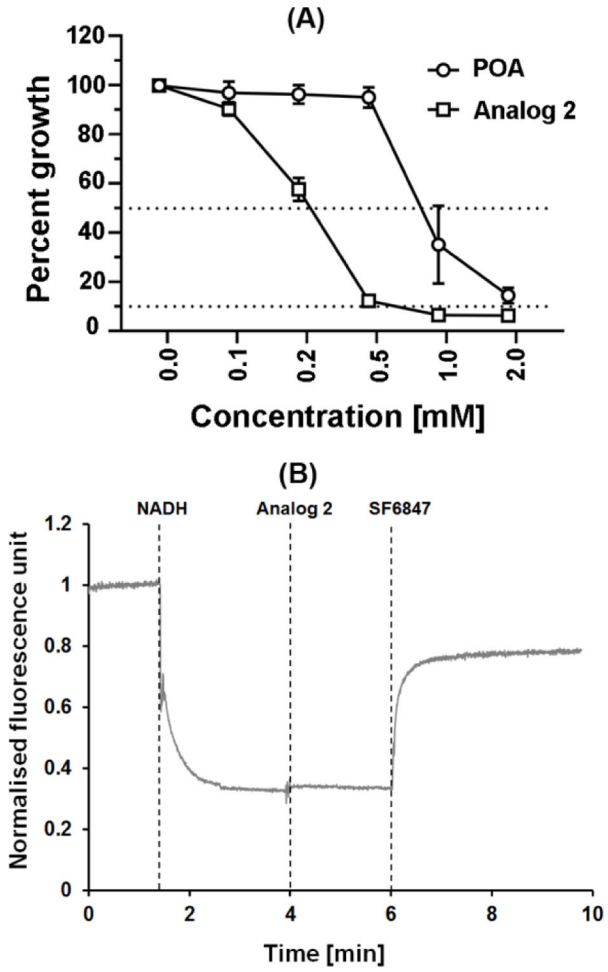

Figure 7:

(*A*) Activity of pyrazinoic acid (POA) and analog 2 against *M. bovis* BCG. Growth inhibition dose-response curves are shown. Exponential phase cultures (OD_{600} = 0.05) were treated with increasing concentrations of POA or analog 2 for 5 days and growth was measured by OD_{600} determination. Experiments were carried out three times independently in duplicate. Mean values and standard deviations are shown. Activity of analog 2 was also confirmed for *M. tuberculosis* H37Rv (MIC_{50} = 1000 μM). (*B*) Effects of analog 2 on the transmembrane pH gradient of IMVs prepared from *M. smegmatis* plasma membranes. Shown is the effect of 1 mM of analog 2 on the quenching of fluorescence of the pH-sensitive fluorophore ACMA. At the beginning of the experiments 2 mM NADH was added as an electron donor to the vesicle samples. The inverted vesicles oxidized NADH and pumped protons to generate the transmembrane pH gradient, visualized as quenching of fluorescence; 1 μM uncoupler SF6847 was added at the end of each experiment as a positive control to collapse the transmembrane pH gradient. The vertical dotted lines indicate the time points at which NADH, analog 2 or SF6847 was added. The experiments were carried out twice independently, showing the same result. Data from a representative replicate are shown.

Table 1:

Characterization of 3-Substituted POA Analogues

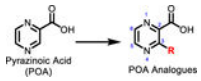

Compound	*Structure*	K_D *(μM)*	*Compound*	*Structure*	K_D *(μM)*
POA	-	20 ± 0.2	**10**		286 ± 17
1	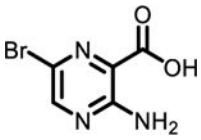	14 ± 0.9	**11**	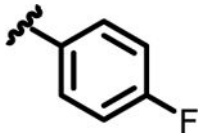	550 ± 20
2	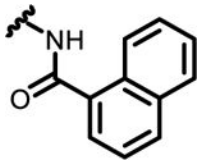	20 ± 0.5	**12**	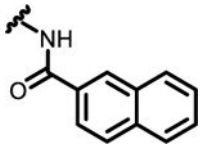	N.d.[b]
3	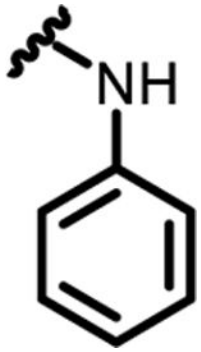	27 ± 2.5	**13**	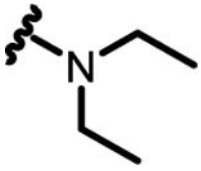	No binding
4		40 ± 1.8	**14**	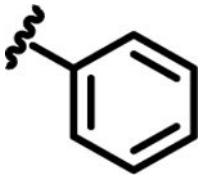	No binding

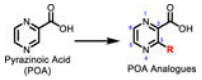

Compound	*Structure*	*K_D (μM)*	*Compound*	*Structure*	*K_D (μM)*
5	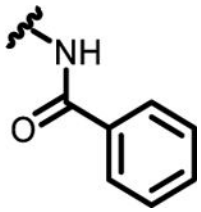	50 ± 3.2	**15**	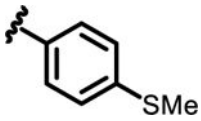	No binding
6	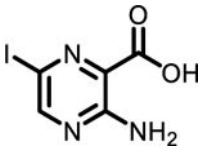	100 ± 4.8	**16**	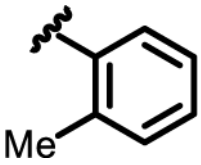	No binding
7	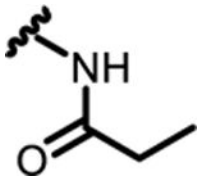	200 ± 0.9	**17**	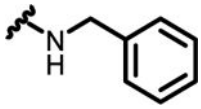	No binding
8	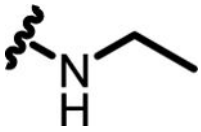	200 ± 2.1	**18**	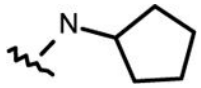	No binding
9	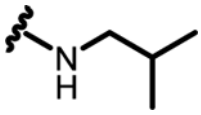	265 ± 4.5			

[a] Binding constant determined by ITC,

[b] Compound was insoluble at 10 mM in DMSO and binding could not be determined.